JOURNAL OF MECHANICAL ENGINEERING AND SCIENCES (JMES)
ISSN: 2289-4659 e-ISSN: 2231-8380
VOL. 16, ISSUE 3, 9066 – 9080
DOI: https://doi.org/10.15282/jmes.16.3.2022.09.0718

ORIGINAL ARTICLE

Experimental investigation of aerodynamics behavior of a new generic of unmanned air vehicle (heliplane)

Kaddouri Djamel[1,2], Benlefki Abdelkrim[3], Adjlout Lahouari[2], Mokhtari Abdellah[2]

[1] Superior School of Electrical and Energetic Engineering of an (ESGEEO), Chemin Vicinal N9, 31000, Oran, Algeria.
Phone: +213 041 240 937; Fax.: +213 041 240 639
[2] Lahn Laboratory, University of Sciences and Technology Oran MB, BP1505, ElM'naouer, 31000 Oran, Algeria.
[3] Lma Laboratory, University of Sciences and Technology Oran MB, BP1505, ElM'naouer, 31000 Oran, Algeria.

ABSTRACT – The aeronautics studies and particularly the development of drones represent an important field, in which there is a very large number of research and studies.This article aims to present an experimental aerodynamic study of an autonomous surveillance unmanned aerial vehicle (UAV) that is capable of combining the advantages of both categories, namely the fixed-wing drones and the rotary-wing drones. To achieve this objective, a wind tunnel was used to study the flow around this drone in order to better understand the aerodynamic phenomena and to obtain some initial estimates of the lift, drag and moment coefficients, at three different Reynolds numbers of 4.02×10^4, 6.03×10^4 and 8.04×10^4, and for different angles of attack, from [−45°, +45°] with step of 1°.The experimental results obtained in this work show an casi-symetrical variation bertwen the negatif and positif incidence angles of the lift coeffecient, wiche indicate that the heliplane can fly in an inverted position, whatever the angle of incidence. Moreover, the minimum mean value of drag coeffecient according 1° incidence angle is 0.0478 then the drag due to geometry and pitching moment can never be canceled.

ARTICLE HISTORY
Received: 19th Apr. 2022
Revised: 13th Aug. 2022
Accepted: 01th Sept. 2022

KEYWORDS
Drag
Experimental
Aerodynamics
Flight mechanics
Lift
UAV
Wind tunnel test

INTRODUCTION

Over the last few years, scientific research and technological advancements in aeronautics have made it possible to predict a significant progress in air vehicles which are becoming increasingly more efficient and above all capable of evolving autonomously. This challenge would involve many improvements in several disciplines. It is widely acknowledged that the field of unmanned aerial vehicles has been much investigated during the last decade, and has attracted the interest of many researchers working in disciplines particularly related to automation [1-5] electronics [6-8], mechanics and aerodynamics [9-11]. Drones or UAVs are unmanned flying vehicles capable of carrying out a mission in autonomy or semi- autonomous. Their main use is military for reconnaissance or surveillance missions, without the risk of life loss [12, 13]. Indeed, they are well suited for carrying out missions that would potentially put a crew in danger, or that requires a permanence on an area that would be tedious for a crew on board [14]. Their use began with everything related to observation and then expanded to the acquisition of objectives as well as electronic warfare, and the destruction of targets. Civil applications are emerging, such as highway traffic monitoring, forest fire prevention, weather data collection and inspection of engineering structures [15]. The size of the drones varies from centimeter to several meters [16-19], as does their mode of propulsion that evolves according to needs. There are two types of wings: fixed wings for flight in advance mode and rotating wings for hovering [20, 21]. Indeed, different configurations of drones have been proposed so far. It should be mentioned that rotary-wing vehicles have a major advantage over fixed-wing vehicles, especially in an environment where the capacity to hover is important.

Furthermore, a very large number of researchers have experimentally and numerically investigated the aerodynamic performance of drones of various shapes and tried to develop techniques for improving this performance even more. For example, S. Sudhakar et al [22]conducted an experimental study on unmanned aerial vehicles with three types of wings. The first drone had single wings, the second one was provided with wings with tubercles of constant wavelength and amplitude along the wingspan, and the third one possessed tubercles of varying amplitude and wavelength along the span. The present work sought to show that the incorporation of tubers on the leading edge of a generic UAV wing made it more stable throughout the range of operations and enhanced its aerodynamic performance. Zhe Hui et al [23] carried out another experimental study in which the simultaneous imitation of postures and wing surface of a pigeon were designed and tested; also, the aerodynamic performance of the UAV with different wing configurations was investigated in detail. In addition, two wing configurations of continuous structures and different shapes were designed as comparative models to be used in wind tunnel experiments. The results obtained showed that the drone can still maintain an optimal lift-to-drag ratio. In addition, the asymmetric morphing of the wing allows for a good command of the UAV rotation. It should be noted that compared with a continuous wing surface structure, the bio-inspired discrete wing surface structure cannot only diminish the UAV induced drag by effectively decreasing the wing tip vortices but also improve the lateral-directional stability of the UAV. In the same context, Dae-Kwan Kim et al [24] designed and aerodynamically tested a

*CORRESPONDING AUTHOR | Kaddouri Djamel | ✉ kaddouridjamel78@gmail.com

smart flapping wing in a subsonic wind tunnel. The experimental results indicated that the effect of the camber engendered by the MFC (macro-fiber composite) developed a sufficient aerodynamic advantage. It should be noted that the flexibility of the wing in the direction of the chord is one of the most important parameters affecting the aerodynamic performance; in addition, the lift produced under near-constant flow conditions is mainly affected by the forward speed and effective angle of attack.

It is worth recalling that a lot of researchers have preferred to study the performance of new drones using numerical simulations in addition to experimental wind tunnel testing. Jeong-Hyun Cho [25] investigated numerically and tested the power-up effect of a thrust propeller unmanned aerial vehicle in a wind tunnel; the results showed that the most important power-up effect is to produce the aircraft's wake drag and nose-up pitching moment. Therefore, the power-up effects tend to diminish the performance as well as the longitudinal stability of the aircraft with a thrust propeller. It should be noted that the power-up effect is more pronounced at slower speeds and at higher thrust levels. For their part, Warda Boudaoud et al [26] used the computational fluid dynamics (CFD) and the wind tunnel to investigate the effect of an external vortex around an unmanned aerial vehicle in order to obtain initial estimates of lift and drag coefficients, with a Reynolds numbers of 3,85 106, for various angles of attack. The findings suggested that the influence of the vortex was quite significant around the drone, and the instability phenomena around the roll axis werevisible.

Furthermore, several works on design and realization of drones were reported in the literature. For example, Abdelwahid Boutemedjet et al [27] studied and presented in their papers the aerodynamic design procedure of a mini unmanned aerial vehicle, intended for aerial reconnaissance at low altitude with a small Reynolds number. The parameters of the wing plane were determined using an aerodynamic optimization procedure based on genetic algorithms and artificial neural networks. This design study was followed by a detailed aerodynamic analysis using the panel method. Moreover, some fluid dynamics simulations and wind tunnel tests were also carried out. Pedro David Bravo-Mosquera et al14, pre-sented a research study that targeted the aerodynamic design of a low cost unmanned aerial vehicle (UAV) capable of performing aerial surveillance of volcanic environments. The findings indicated that the entire design process was quite coherent because the analytical, numerical and experimental results were very similar with respect to the coefficient of lift C_L and coefficient of drag C_D. In addition, the characteristics of the drones were within the limits of the design requirements. Note that these drones have several aerodynamic and performance advantages over other vehicles used for the same purpose. This suggests that, on a large scale, the aerodynamic behavior of the drone is appropriate for performing the mission it was designed for. However, real environmental studies are still needed for the purpose of validating the reliability of the newly designed drone.

The present work aimed to develop an unmanned aerial vehicle (UAV), i.e. the quadrotor, which was then named heliplane. This study primarily concentrated on the aerodynamic analysis of the uav in order to find its most optimal geometric shape. The aerodynamic coefficients were then determined by carrying out several experimental tests in order to realization this uav or drone. The main idea of this theme can be summed up in the design of a surveillance drone characterized by a special ability, compared to other drones, which is the ability to fly in different directions with more flexibility and stability, this characteristic is ensured by the combination between the velocities of the four propellers, the different movements are well detailed in the paragraph below.

It is useful to recall that the heliplane is an automatic, rotary-wing aerial vehicle. It is made of three propellers: two vertical and two horizontal; they are driven by direct current motors or brushless motors using a reduction gear. In addition, two propellers (1 and 2) are mounted vertically on the fuselage to help the heliplane to fly vertically and to hover, like helicopters. Two other propellers (3 and 4) are mounted on the wings to help the drone fly like an airplane, as shown in Figure 1.

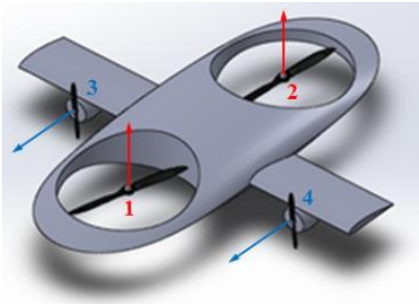

Figure 1. Heliplane with propellers

This type of structure allows the heliplane to move in all directions. The choice of this system in the present study was mainly motivated by the advantages it presents over a conventional airplane or even a helicopter. It is especially worth mentioning:

- The vertical takeoff and landing, and hover like a helicopter [28-30],
- A behavior similar to that of an airplane [31]; this vehicle can move very quickly while consuming little energy,
- The simple mechanical structure,
- The important payload,

- Large propellers are not required,
- Possibility of making left and right maneuvers while keeping the same direction,
- In the steady state, the gyroscopic couples, which are considered as the greatest source of non-linearity in the system, are zero.

Furthermore, the structure proposed in this study allows the heliplane to move in all directions as follows:

- Increase and decrease the velocity of the two vertical propellers (1 and 2) at the same time, which causes a displacement along the z- axis.
- Increase and decrease the velocity difference between the two vertical propellers (1 and 2), which generates a pitching moment with a displacement along the x-axis (a slight yaw motion occurs due to coupling).
- Increase the velocity of the two horizontal propellers (3 and 4) at the same time, which causes a displacement along the x-axis.
- Increase and decrease the velocities of the two horizontal propellers (3 and 4), which generates a yaw with a displacement along the y- axis (a slight rolling movement occurs due to coupling).
- Combination of the velocities of all three propellers allows the heliplane to take any direction

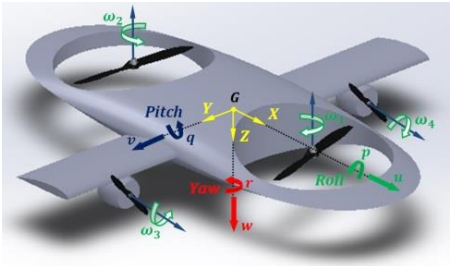

Figure 2. Motions description of the heliplane

The paper is outlined as follows. Experimental setup, model design and the force measurement are presented in section 2. Results of the heleplane aerodynamic coefficients are given in section 3 with discussion. Performance comparisons of the heleplane with others unmanned aerial vehicles are presented in section 4. Finally, Section 5 presents some conclusions and future works.

EXPERIMENTAL WORK

In this part, the experiments were carried out on a proto-type reduced to 40% of the heliplane model which is explicitly detailed in the next section. These experiments are be carried out using a subsonic wind tunnel of type TE44, with a total length, width and height of 7400 mm, 3320 mm, and 1850 mm, respectively, for the purpose of better detecting the aerodynamic phenomena, as shown in Figure 3, in addition to a TE81 balance. The wind tunnel is characterized by a maximum air velocity of 60 m/s in a closed circuit and a square section test duct of dimensions 457 x 457 mm and a length of 1200 mm. The TE81 balance is free to rotate 360° for adjusting the angle of incidence of the model, while its position can be locked using an inci-dence clamp. This balance is equipped with the DATA Slim software that is intended to measure the three aerodynamic quantities, namely the drag, lift and pitching moment.

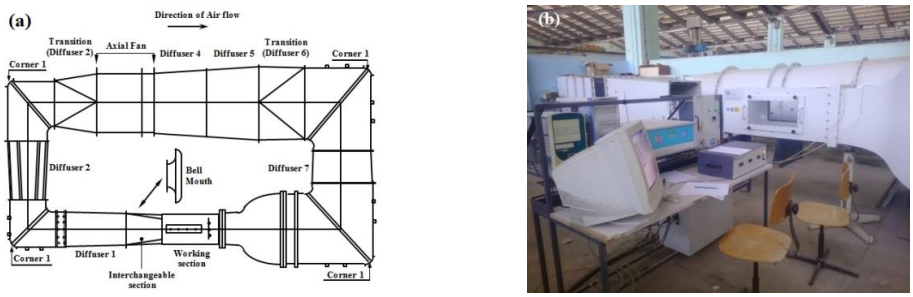

Figure 3. (a) Operating diagram of the wind tunnel and (b) Wind tunnel

Model Design

The selection of the geometric shape of the drone depends primarily on its expected performance, good lift and minimum fall speed, maximum finesse and minimal energy consumption. All these priority conditions pushed the

researcher to achieve aerodynamic shape optimization with low drag. The geometric modeling was performed using the SOLIDWORKS software (Figure 4).

Figure 4 shows the Clark Y profile used for wings; it is a plano-convex profile, very often called a flat profile by model makers. This type of profile, which is the one that was used on the first airplanes, has very high lift from low incidences, and medium drag. However, the center of gravity of this profile tends to shift. It is extensively utilized in model making because it is easy to build and gives with low drag. The geometric modeling was performed using the SOLIDWORKS software (Figure 4).

Figure 4 shows the Clark Y profile used for wings; it is a plano-convex profile, very often called a flat profile by model makers. This type of profile, which is the one that was used on the first airplanes, has very high lift from low incidences, and medium drag. However, the center of gravity of this profile tends to shift. It is extensively utilized in model making because it is easy to build and gives good results. At the angle of 0°, this profile shows a coefficient of lift of 0.26, which is relatively high, and a fairly average drag coefficient equal to 0.017. The relative thickness of a Clark Y profile is about 11.68%, with a very small camber of about 2.7%; its maximum fineness is about 16.9 for an angle of incidence of 4°.

The present work aimed to develop an autonomous flying machine, i.e. the quadrotor, which was then named heliplane. This study primarily concentrated on the aerodynamic analysis of the machine in order to find its most optimal geometric shape. The aerodynamic coefficients were then determined by carrying out several experimental tests in order to realization this flying machine or drone.

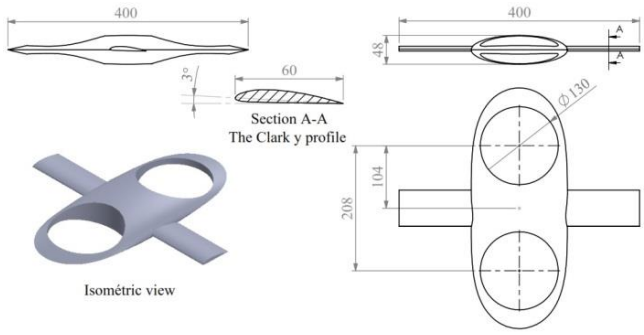

Figure 4. Heliplane description (dimensions in mm)

A wooden prototype was designed from drawings generated by SOLIDWORKS for the purpose of performing wind tunnel testing of the heliplane. This prototype was handcrafted in wood (the easiest material to handle) with a scale of 1/25 so to have a wingspan of 400 mm which corresponds to the maximum width of the test vein of the wind tunnel. The shape of each part of the structure was modified until the desired shape was obtained. The table below summarizes the different steps required to design the drone. Indeed, the first step consists of cutting out the main parts of the heliplane. The second step was to shape the three parts in an artisanal way. Then, the third step concerned the assembly of all three parts. Afterwards, the entire surface was coated with an automotive sealant and then painted with two metallic paint layers to make it smoother (Figure 5).

Figure 5. Final geometry of the heliplane

Force Measurement

The TE81 balance used in the experimental tests represents a support system for the wind tunnel models; it suits quite well the test stream of the TE44 wind tunnel and fits the profiles as well, as illustrated in Figure 6. This balance is intended to measure three main forces exerted on the model; these are the lift, drag and pitching moment forces. Furthermore, the models to be used with the balance must be fitted with a 220 mm long mounting rod which must be inserted into the bore of the model support; it is graduated around the periphery. It is free to rotate 360° in order to adjust the incidence angle of the model; however, its position can be locked using an incidence clamp. In addition, the forces acting on the force plate are transmitted through flexible cables that are connected to the strain gauges of the load cells. These devices are

intended for measuring the vertical forces (AFT, FORE) and the advance resistance force (DRAG). A display device, with three displays, shows the charge of each cell.4).

1. DRAG gives the drag force N,
2. The sum of AFT and FORT gives the lift force N,
3. Once multiplied by 0.127, the difference between AFT and FORT gives the moment N.m.

Figure 6. Balance TE81

Once the design phase of the experiment completed, the essential step of sensor calibration takes place for the experimental realization of this work. The functioning of these force sensors is based on the principle of the modification of internal resistance when a force is applied to its ends, as clearly shown in Figure 7. The vertical sensors used are Sensy 2712 s type possessing a sensitivity of 1.93 (m V)/V for a maximum load of 10 kg. However, the sensor used for drag measurement is slightly different; it is a TML Tokyo Sokki TCLZ-10KA sensor that has a sensitivity of 1.5 (m V)/V for the same maximum load of 10 kg.

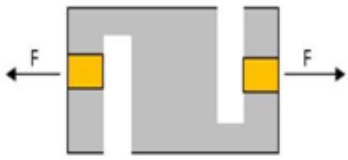

Figure 7. Force sensor

The DATA Slim application software is supplied with the TE81 balance; it is primarily intended to record the acquired data. It offers the researcher the possibility of using other instruments, which are supplied with the wind tunnel, and that are supposed to facilitate the experiment, as illustrated in Figure 8. Among these instruments, it is worth citing the pressure sensor (TE44 DPS) that has 20 channels, which are used to capture static pressures, by connecting them to the pressure ports of the models. This sensor also includes two independent channels intended to capture the static and local pressures. The pressure sensor is also connected to the balance through a cable. To allow direct reading on the PC, the Data Slim software installed and the data are saved in extension files. In addition, the software interface displays successfully all three quantities, i.e. DRAG, AFT and FOR, the total and static pressures, and the pressures of the 20 channels one after the other.

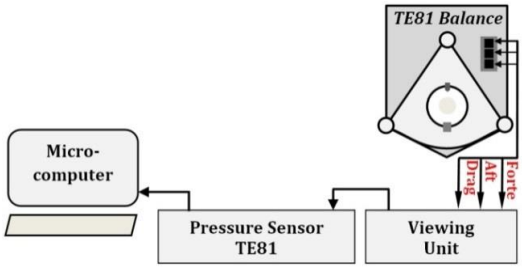

Figure 8. Connection of the balance to the microcomputer

In this experimental study, the heliplane was tested with three Reynolds numbers, i.e. 4.02×10^4, 6.03×10^4 and 8.04×10^4, in order to determine the lift and drag coefficients. The angles of attack explored are within the range [−45°, +45°], with a step increment of 1°, in order to collect as much in-formation as possible. The experiment was carried out in the TE44 wind tunnel according to the following pattern:

1. Calibration of the balance;

2. Fixing of the heliplane on the balance in such a way that this heliplane is opposite the flow. This corresponds to the angle 0° (Figure 9).
3. Turn on the wind tunnel.
4. Record the heights (in mm H_2O) of the total, static and reference pressure at the inlet of the test section.
5. Calculate the flow velocity using Equation 1.
6. Vary the azimuth angle from +45° to −45° with a step of 1° by means of the azimuth angle adjuster.
7. Record the values of the forces AFT and FOR.

$$\Delta H = \frac{U_{\infty}^2 . \rho_{air}}{2 . g . \rho_{eau}} \tag{1}$$

$$\rho_{air} = \frac{P_{atm}}{R . P_{atm}} \tag{2}$$

Where ρ_{eau} = 1000 k/gm^3 is the water density and gas constant R = 287 (J/KG) K°.

Before proceeding with the experiment, measurements were performed on the stinger alone, without the reduced model, in order to subtract them from those made on the whole system (stinger + drone), and then deduce the forces acting on the drone only. The measurements on the stinger were carried out for a null incidence because the same results are obtained and little variation was observed for the other incidences.

Figure 9. Fixation of the heliplane

Calculation of the Drag Coefficient

The drag force of the drone is obtained by subtracting the stinger drag from the drag obtained in the wind tunnel.

$$F_{Dd} = F_{D\,wt} - F_{Ds} \tag{3}$$

Where F_{Dd} is the drag force of the drone N, F_{Dwt} is the drag force obtained in the wind tunnel N and F_{Ds} is the drag force of the stinger alone. The drag coefficient is then calculated from the following equation:

$$C_D = F_D / \frac{1}{2} \rho V^2 S \tag{4}$$

Calculation of the Lift Coefficient

Likewise for the lift of the F_{Ld}, the value of the lift of the dart lift value is subtracted from that provided by the database of the wind tunnel.

$$F_{Ld} = F_{Lwt} - F_{Ls} \tag{5}$$

$$F_{L\,wt} = AFT + FORE \tag{6}$$

Where F_{Ld} is the lift force of the drone N, F_{Lwt} is the drag force obtained in the wind tunnel N and $F_{L}s$ is the drag force of the stinger alone. The drag coefficient is then calculated from the following equation:

$$C_L = F_L / \frac{1}{2} \rho V^2 S \tag{7}$$

Calculation of the Pitch Moment Coefficient

The pitching moment is given as:

$$M = F_L 0.127 \tag{8}$$

Where M is the pitching moment, and the value 0.127 represents the wind tunnel lever arm. The pitching moment coefficient is therefore calculated from the following equation:

$$C_M = M/\frac{1}{2}\rho V^2 S\, c \tag{9}$$

Where C_M is the moment coefficient of the drone, M is the moment of the drone Nm and c is the average aerodynamic chord. c is equal to the wing chord.

RESULTS AND DISCUSSIONS

In this experimental study, the heliplane was tested with three Reynolds numbers Re = 4.02×10^4, 6.03×10^4 and 8.04×10^4 in order to determine the lift, drag and pitching moment coefficients. In order to collect as much information as possible, the range of attack angle explored was taken within the range [−45°, +45°] with a step increment of 1°. Where C_M is the moment coefficient of the drone, M is the moment of the drone Nm and c is the average aerodynamic chord. c is equal to the wing chord.

Lift Coefficient

The variation of the coefficient of lift C_L as a function of the angle of incidence of the heliplane is shown in Figure 10. The shapes of the three curves corresponding to the three Reynolds numbers are the same with a maximum and minimum defrence of 0.03 and 0.0024 for 31° and -9° respectively , and the results obtained from the wind tunnel tests indicate that, for example, the drone stalls at the angle of 31° for Re = 8.04×10^4 and the corresponding coefficient of lift is equal to 0.2745. For the other two Reynolds numbers, the results are presented in Table 1. Furthermore, Figure 10 also makes it possible to determine the maximum coefficient of C_{Lmax} and the corresponding angle.

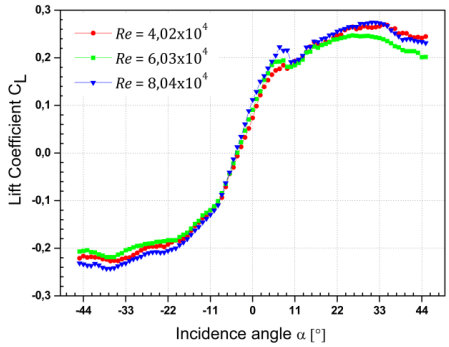

Figure 10. Lift coefficients C_L as a function of the angle of incidence α

Table 1. Lift curve parameters

Re	$C_{L\alpha=0}$	C_{Lmax}	$\alpha_{C_{Lmax}}$
4.02×10^4	0,0737	0,2664	29°
6.03×10^4	0,0907	0,2460	30°
8.04×10^4	0,1117	0,2745	31°

It is well noted that the curve in Figure 10 is quasi linear between the values of angles of attack between −10°/8°, −10°/8° and −10°/7 for the Reynolds numbers Re = 4.02×10^4, 6.03×10^4 and 8.04×10^4, respectively. Moreover, the slope for each Reynolds number was taken from Table 2. It should also be noted that from the shape of the curve is not linear after the stall angle.We also note Beyond the stall angle, there is nevertheless an increase in the lift coefficient for the three Reynolds, then a sudden drop;the flow no longer follows the shape of the profile.In addition, the coefficient of lift (C_L) is not zero for the angle of incidence α = 0, for all three velocities due to the type of profile used for the wings. It should be recalled that this is in fact a Clark Y profile which is weight-bearing even at low incidence.

Table 2. Different slopes for the three Reynolds numbers

Re	4.02×10^4	6.03×10^4	8.04×10^4
Slope	0,0171	0,017	0,0201

The curve of the lift coefficient for Re = 8.04×10^4 in figure 10, they show that, even with a negative angle of attack, the helipad is stable and produces lift at -4°.Then, the lift coefficient increases almost linearly with angle of attack and stalls at +7° where it decreases to +12.Then it increases with angle of attack and reaches a maximum of +31° where it decreases for the second time. The flow no longer follows the shape of the profile;this is the stall phenomenon.

It should be noted that beyond the stall angle, there is still an increase in the lift coefficient for all three flow regimes. The values of C_L in the negative part are quite large, which gives the heliplane the ability to fly in an inverted position.

Drag Coefficient

The variation of the drag coefficient C_D as a function of the angle of incidence α of the heliplane is shown in Figure 11 which shows that the profile is parabolic and does not intersect the incidence axis. The shapes of the three curves corresponding to the three Reynolds numbers are the same with a maximum and minimum defrence of 0,0227 and 0.0013 for 35° and 13° respectively. Indeed, the form drag is never zero whatever the angle of incidence. Moreover, one may note a small dispersion of the drag curves for the three Reynolds number: 4.02×10^4, 6.03×10^4 and 8.04×10^4.

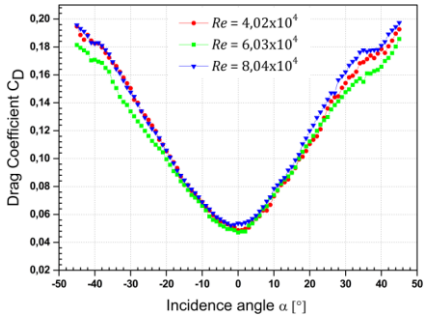

Figure 11. Drag coefficients C_D as a function of the angle of incidence α

This Figure 11 shows that the drag is affected by the fuselage, and an almost linear increase in drag is observed as the heliplane stalls due to the separation of the boundary layer from the upper surface of the drone. In order to move with minimum drag, the drone should have an angle of incidence successively equal to 1°, 1° and −2° corresponding respectively to the Reynolds numbers 4.02×10^4, 6.03×10^4 and 8.04×10^4. The drag curve parameters are summarized in Table 3.

Table 3. Drag curve parameters

$\boldsymbol{Re}$	$\boldsymbol{C_{Dmin}}$	$\boldsymbol{\alpha_{C_{Dmin}}}$
$4,02\times10^4$	0,0486	1°
$6,03\times10^4$	0,0470	1°
$8,04\times10^4$	0,0522	-2°

The minimum drag coefficient related to the wetted surface of the obstacle was compared to the friction coefficient of the flat plate, at zero incidence, in the case of a laminar boundary layer and a turbulent boundary layer, in order to know the boundary layer that develops around the heliplane. In this case, two formulas were used:

1. Friction coefficient of a laminar boundary layer.

$$C_{FL} = {}^{1,327}/_{\sqrt{Re}} \tag{10}$$

2. Friction coefficient of a turbulent boundary layer

$$C_{FT} = {}^{0,075}/_{(\log_{10} Re - 2)^2} \tag{11}$$

3. Drag coefficient

$$C_{Dmin} = C_{Dmin}\frac{S_{FP}}{S_m} \tag{12}$$

Where S_{FP} = 0.04392 m^2 is the planar surface and S_m = 0.11920 m^2 is the wetted surface. The results of this comparison are shown in Table 4. Close examination of the values reported in Table 4 shows that the hypothesis of an entirely turbulent boundary layer around the obstacle is justified.

Table 4. Comparison between the laminar and turbulent friction coefficients and the drag coefficient

Re	C_{FL}	C_{FT}	C_{Dmin}
4,02×10^4	6,6192×10^{-3}	11,0596× 10^{-3}	17,8988× 10^{-3}
6,03×10^4	5,4045 ×10^{-3}	9,7030× 10^{-3}	17,3095× 10^{-3}
8,04×10^4	4,6805 ×10^{-3}	8,8863× 10^{-3}	19,2246× 10^{-3}

Polar

The experimental tests made it possible to determine the actual polar of the drone. The results obtained are represented in Figure 12. The same shapes of the three curves of polar is observed for the Reynolds numbers cases under study with little deference, as it is shown in this figure. After the stall angle, the variation of C_D as a function of C_L is almost linear.

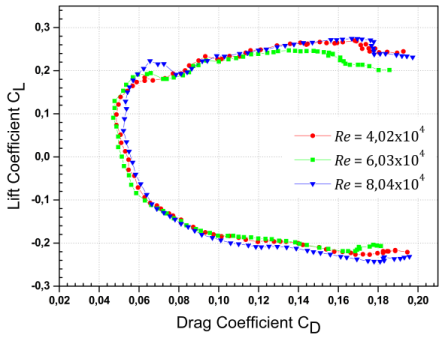

Figure 12. Polar for the three Reynolds numbers

Close examination of the polar allows obtaining useful information, as illustrated in Table 5.

Table 5. Polar parameters

Re		C_D	C_L	α
4,02×10^4	C_{Dmin}	0,0486	0,0737	0°
	$C_{DC_{Lmax}}$	0,1507	0,2664	29°
6,03×10^4	C_{Dmin}	0,0470	0,0907	0°
	$C_{DC_{Lmax}}$	0,1475	0,2460	30°
8,04×10^4	C_{Dmin}	0,0522	0,0607	-2°
	$C_{DC_{Lmax}}$	0,1667	0,2745	31°

Fineness

Figure 13 depicts the variation of the ratio C_L/C_D as a function of the angle of incidence of the heliplane. The shapes of the three curves corresponding to the three Reynolds numbers are the same with a maximum and minimum defrence of 0.5879 and 0.0158 for 7° and -9° respectively. Examination of this figure made it possible to identify the maximum fineness of the drone and the cruising angle, for each Reynolds numbers. The results obtained are shown in Table 6.

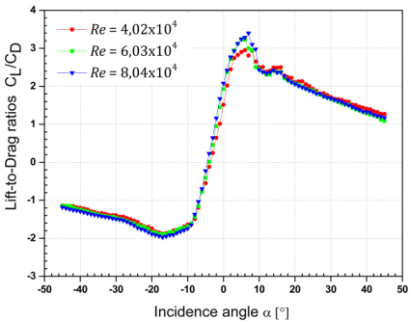

Figure 13. Fineness curve

Table 6. Optimal flight path angle and maximum finesse

Re	C_L/C_D	α	C_L	C_D
4,02×10⁴	2,9503	6°	0,1734	0,0588
6,03×10⁴	3,2435	6°	0,1846	0,0569
8,04×10⁴	3,3998	7°	0,2227	0,0655

Pitch Moment

The pitching moment was calculated with respect to the center of symmetry of the plane shape (CSPS) of the heliplane, while referring to its surface and the chord of the wing.

Variation of C_M as a function of α

The first study investigated the evolution of the pitching moment coefficient C_M as a function of the fuselage angle of attack as shown in Figure 14. Examination of the figure above indicates that for zero fuselage angle of attack, the moment coefficient is equal to zero, which means that the drone is subjected to a nose-up pitching moment because it is positive.

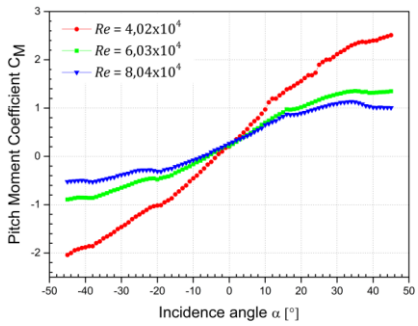

Figure 14. Pitching moment coefficients C_M as a function of the angle of incidence α

It is worth noting that it is also possible to determine through this curve the angle corresponding to a zero pitching moment. The values of this moment are given in Table 7.

Table 7. Parameters of the pitching moment coefficient curve as a function of the angle of attack α

Re	α	$C_{M\alpha=0}$	C_M	$\alpha_{C_M=0}$
4,02×10⁴	0°	0,0810	0	-3.5°
6,03×10⁴	0°	0,0848	0	-6°
8,04×10⁴	0°	0,1069	0	-7°

Variation of C_M as a function of C_L

The second study concentrated on the evolution of this same coefficient as a function of the lift coefficient, as depicted in Figure 15

The equation which governs the approximation of the linear part of the experimental results is given as:

$$C_{MF} = A + BC_L \tag{13}$$

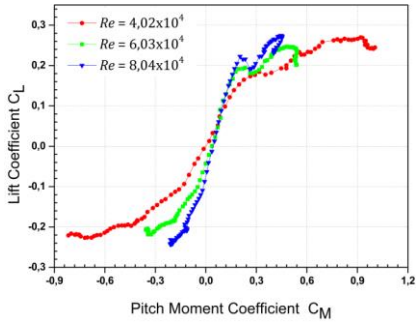

Figure 15. Evolution C_M as a function of C_L

The results corresponding to Re = 8.04×10^4, presented in Figure 16, were used to discuss the evolution of the pitching moment coefficient as a function of the lift coefficient.

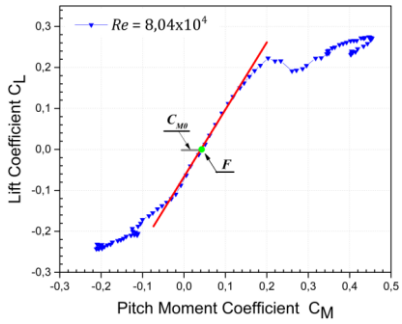

Figure 16. Evolution of C_M corresponding to Re = 8.04 10^4 as a function of C_L

It is clear that the curve is almost linear for the C_L values between -0.1202 and 0.2227 and for those of C_{MF} between -0.0308 and 0.2028. The equation for linear interpolation, in red in Figure 16, is given by:

$$C_{MF} = -0{,}05627 + 1{,}44942C_L \tag{14}$$

The values of the pitching moment coefficient corresponding to zero lift coefficient C_{M0}, as well as the slopes of lines B for all three Reynolds numbers, are reported in Table 8.

Table 8. Parameters of the curve representing the pitching moment coefficient as a function of the lift coefficient

Re	***A***	***B***
4.02×10^4	0,0154	0,5732
6.03×10^4	-0,0161	1,0331
8.04×10^4	-0,0562	1,4494

Power Coefficient

Figure 17 displays the evolution of the power coefficient C_P as a function of the angle of attack. The shapes of the three curves corresponding to the three Reynolds numbers are the same with a maximum and minimum defrence of 0.4225 and 0.0112 for 7° and -9° respectively. The power coefficient is calculated from the following equation:

$$C_{Pr} = {C_D}/{C_L^{3/2}} \tag{15}$$

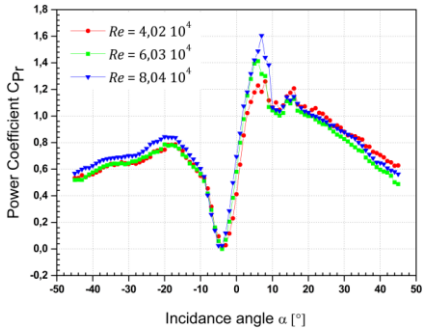

Figure 17. Evolution of C_{Pr} as a function of α

The values of the power coefficient C_{Prmax} for the cases under study are presented in Table 9.

Table 9. Maximum power coefficient C_{Prmax}

Re	***α***	$C_{Pr\,max}$	C_L
4.02×10^4	6°	1.2288	0.17347
6.03×10^4	6°	1.4119	0.19162
8.04×10^4	7°	1.6046	0.22275

COMPARISON

The heliplane was compared with three other uav's to evaluate aerodynamic performance. Two types of configuration were chosen for comparison, the fixed-wing and the rotating wing drone, presented in Figure 18. All chosen drones for comparison are roughly equal in Reynolds number. The first drone chosen is a catapult-launched tandem wing morphing unmanned aerial vehicle[32] (Team 1), the second is a fixed wing micro air vehicle (MAV) [17] (Team 2) and the last drone is a rotating wing micro air vehicle [16] (Team 3).

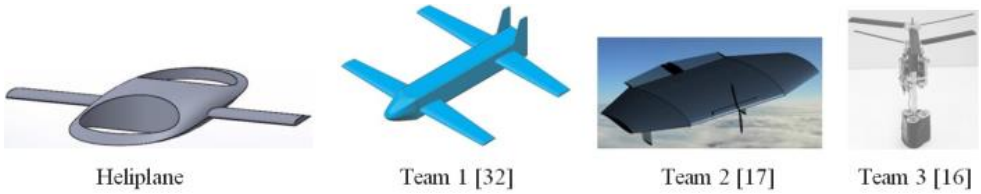

Figure 18. The chosen drones for comparison

Figure 19 and 20 presents the aerodynamic coefficients, the lift end drag coefficients, based on the experimental results. Moreover Table 10 presents the key features aerodynamic of each of the concepts. Namely, the maximum lift coefficient C_{Lmax}, minimum Drag coefficient C_{Dmin}, maximum Lift-to-Drag ratios$(C_L/C_D)_{max}$, main wing span and airfoil are shown.

Table. 10. Key features aerodynamic of each of the concepts

	Re	C_{Lmax}	C_{Dmin}	$\left(\frac{C_L}{C_D}\right)_{max}$	Wing span or propeller length	Wing airfoil or propeller airfoil
Heliplane	8.04×10^4	0,2745	0,0522	3,3998	0.4 m	Clark y
Team 1	1×10^5	0,8204	0,0455	6,84896	0.64 m	Ritz 3-30-11
Team 2	8.7×10^4	0,30453	0,0392	2,73538	0.224 m	S5010
Team 3	6×10^4	1,1821	0,0874	15,1579	0.07 m	Curved plate airfoils

The variation of the drag coefficient as a function of the angle of attack is presented in Figure 19, this figure represents a comparison of the results of the experimental measurements of the drag of the present heliplane and three other unmanned aerial vehicles. This figure clearly shows that the new aerial vehicle studied in the present work, named heliplane, has a remarkable advantage of a very low aerodynamic drag, particularly for low incidence angles except for the Team 2 vehicle characterized by a more advantageous drag, this is for the reason of having two holes made on the fuselage which are reserved for the location of the propellers. The difference in drag coefficients between the heliplane and the three geometries is shown in Table 11.

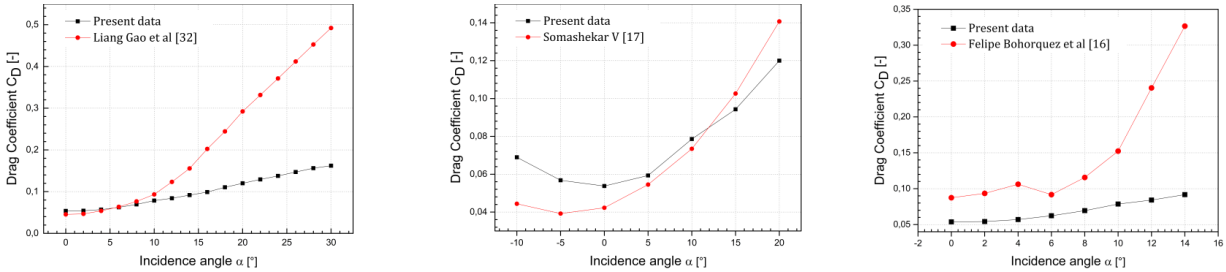

Figure 19. Comparison of the drag coefficient

Table. 11. Difference in drag coefficients between the heliplane and the three geometries

	Max Drag difference		Min Drag difference	
	C_D	α	C_D	α
Heliplane & Team 1	0.3301	30°	0.0011	06°
Heliplane & Team 2	0.0207	20°	0.0083	15°
Heliplane & Team 3	0.2347	14°	0.0294	06°

Regarding the other aerodynamic parameter, Figure 20 shows a comparison of the lift coefficient of the heliplane and the same three air vehicles. It is noted that the lift coefficient of the vehicle of the team1 and of the team3 is more advantageous than the heliplane compared to the vehicles of the team2. The difference in lift coefficients between the heliplane and the three geometries is shown in Table 12.

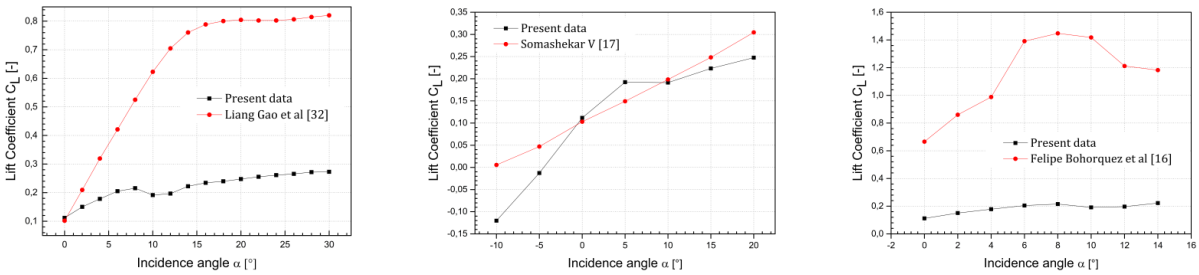

Figure 20. Comparison of the liftg coefficient

Table. 12. Difference in lift coefficients between the heliplane and the three geometries

	Max Lift difference		**Min Lift difference**	
	C_L	α	C_L	α
Heliplane & Team 1	0.5475	30°	0.0099	0°
Heliplane & Team 2	0.0570	20°	0.0070	10°
Heliplane & Team 3	1.2323	8°	0.5539	0°

Here one's must specify that the lift measured for the heliplane is only the aerodynamic lift (C_L) and not the total lift (C_{LTotal}). For this reason, the lift capacities of other unmanned aerial vehicle show superiority compared to the heliplane, but by adding the lift generated by the two propellers (thrusters), (C_{LProp}), undoubtedly the total thrust will become greater than all compared unmanned aerial vehicles.

$$C_{L\,Total} = C_L + C_{L\,Prop} \tag{16}$$

CONCLUSIONS

This paper focused on the study of a new geometry of an surveillance unmanned aircraft, called a heliplane. This study was undertaken with the aim of observing the aerodynamic performance of a heliplane through an experimental study. The concept of designing flying machines is judged as an alternative to digital simulation with the aim of having a possible reduction in the cost of the design.

The experimental tests were carried out in a wind tunnel on the heliplane. This aircraft was tested with three Reynolds numbers of 4.02×10^4, 6.03×10^4 and 8.04×10^4, to determine aerodynamic coefficients. The range of the angle of attack explored varies between -45° and +45°, with an increment of one degree. This experimental study has shown, for example, that beyond the stall angle, there is still an increase in the lift coefficient for thethreeflow regimes. Moreover, the C_L values for negative angles are large, which gives the heliplane the ability to fly in an inverted position. It should also be noted that whatever the angle of incidence, the shape drag is never zero. It was found that for the velocity of 20 m/s, the heliplane stalled at the angle of 7°, which corresponds to a lift coefficient equal to 0.2275, fineness equal to 3.3998 and coefficient of maximum power equal to 1.6046. The study shows, therefore, that the heliplane has good aerodynamic behavior.

NOMENCLATURE

C	Mean aerodynamic chord of the wing.
C_D	Drag coefficient
C_L	Lift coefficient
C_{FL}	Friction coefficient of a laminar boundary layer
C_{FT}	Friction coefficient of a turbulent boundary layer
C_M	Pitching coefficient of the drone
C_{M0}	Pitching moment coefficient corresponding to zero lift coefficient
C_{Pr}	Power coefficient
$CSPS$	Center of symmetry of the plane shape
F_D	Drag force
F_L	Lift force
F_{Dd}	Drag force of the drone
F_{Ld}	Lift force of the drone
F_{Ds}	Drag force of the stinger
F_{Ls}	Lift force of the stinger

F_{Dwt}	Drag force obtained of the wind tunnel
F_{Lwt}	Lift force obtained of the wind tunnel
M	Pitching moment
MFC	Macro-fiber composite
R	Gas constant
Re	Reynolds numbers
S	Area
S_{FP}	Planar surface
Sm	Wetted surface
U_{∞}	Air flow velocity
α	Angle of attack
Δ_h	Flow velocity
ρ	Density
ρ_a	Air density
ρ_{atm}	Atmosphere density
ρ_w	Water density

ACKNOWLEDGMENTS

The author(s) received no financial support for the research, authorship, and/or publication of this article.

REFERENCES

[1] L. Zhou, S. Xu, H. Jin, and H. Jian, "A hybrid robust adaptive control for a quadrotor UAV via mass observer and robust controller," *Advances in Mechanical Engineering*, vol. 13, p. 16878140211002723, 2021, doi: 10.1177/16878140211002723.

[2] K. Djamel, M. Abdellah, and A. Benallegue, "Attitude Optimal Backstepping Controller Based Quaternion for a UAV," *Mathematical Problems in Engineering*, vol. 2016, p. 8573235, 2016/03/03 2016, doi: 10.1155/2016/8573235.

[3] R. Jiao, W. Chou, R. Ding, and M. Dong, "Adaptive robust control of quadrotor with a 2-degree-of-freedom robotic arm," *Advances in Mechanical Engineering*, vol. 10, p. 1687814018778639, 2018, doi: 10.1177/1687814018778639.

[4] R. Zuo, Y. Li, M. Lv, and Z. Liu, "Realization of trajectory precise tracking for hypersonic flight vehicles with prescribed performances," *Aerospace Science and Technology*, vol. 111, p. 106554, 2021/04/01/ 2021, doi: 10.1016/j.ast.2021.106554.

[5] M.-D. Hua, T. Hamel, P. Morin, and C. Samson, "Control of VTOL vehicles with thrust-tilting augmentation," *Automatica*, vol. 52, pp. 1-7, 2015/02/01/ 2015, doi: 10.1016/j.automatica.2014.10.129.

[6] G. Di Rito, R. Galatolo, and F. Schettini, "Self-monitoring electro-mechanical actuator for medium altitude long endurance unmanned aerial vehicle flight controls," *Advances in Mechanical Engineering*, vol. 8, p. 1687814016644576, 2016, doi: 10.1177/1687814016644576.

[7] J. Fu, J.-C. Maré, and Y. Fu, "Modelling and simulation of flight control electromechanical actuators with special focus on model architecting, multidisciplinary effects and power flows," *Chinese Journal of Aeronautics*, vol. 30, pp. 47-65, 2017/02/01/ 2017, doi: 10.1016/j.cja.2016.07.006.

[8] G. Di Rito and F. Schettini, "Health monitoring of electromechanical flight actuators via position-tracking predictive models," *Advances in Mechanical Engineering*, vol. 10, p. 1687814018768146, 2018, doi: 10.1177/1687814018768146.

[9] P. A. S. F. Silva, P. Tsoutsanis, and A. F. Antoniadis, "Simple multiple reference frame for high-order solution of hovering rotors with and without ground effect," *Aerospace Science and Technology*, vol. 111, p. 106518, 2021/04/01/ 2021, doi: 10.1016/j.ast.2021.106518.

[10] T. Stokkermans, L. Veldhuis, B. Soemarwoto, R. Fukari, and P. Eglin, "Breakdown of aerodynamic interactions for the lateral rotors on a compound helicopter," *Aerospace Science and Technology*, vol. 101, p. 105845, 2020/06/01/ 2020, doi: 10.1016/j.ast.2020.105845.

[11] A. Kasem, A. Gamal, A. Hany, H. Gaballa, K. Ahmed, M. Romany, M. Abdelkawy, and M. M. Abdelrahman, "Design and implementation of an unmanned aerial vehicle with self-propulsive wing," *Advances in Mechanical Engineering*, vol. 11, p. 1687814019857299, 2019, doi: 10.1177/1687814019857299.

[12] W. Ganglin, "Key Parameters and Conceptual Configuration of Unmanned Combat Aerial Vehicle Concept," *Chinese Journal of Aeronautics*, vol. 22, pp. 393-400, 2009/08/01/ 2009, doi: 10.1016/s1000-9361(08)60116-8.

[13] R. M. Cummings, S. A. Morton, and S. G. Siegel, "Numerical prediction and wind tunnel experiment for a pitching unmanned combat air vehicle," *Aerospace Science and Technology*, vol. 12, pp. 355-364, 2008/07/01/ 2008, doi: 10.1016/j.ast.2007.08.007.

[14] P. D. Bravo-Mosquera, L. Botero-Bolivar, D. Acevedo-Giraldo, and H. D. Cerón-Muñoz, "Aerodynamic design analysis of a UAV for superficial research of volcanic environments," *Aerospace Science and Technology*, vol. 70, pp. 600-614, 2017/11/01/ 2017, doi: 10.1016/j.ast.2017.09.005.

[15] S. G. Kontogiannis and J. A. Ekaterinaris, "Design, performance evaluation and optimization of a UAV," *Aerospace Science and Technology*, vol. 29, pp. 339-350, 2013/08/01/ 2013, doi: 10.1016/j.ast.2013.04.005.

[16] F. Bohorquez, P. Samuel, J. Sirohi, D. Pines, L. Rudd, and R. Perel, "Design, Analysis and Hover Performance of a Rotary Wing Micro Air Vehicle," *Journal of the American Helicopter Society*, vol. 48, pp. 80-90, 2003, doi: 10.4050/jahs.48.80.

[17] V. Somashekar, "A Computational Investigation of Unsteady Aerodynamics of Insect-Inspired Fixed Wing Micro Aerial Vehicle's 2D Airfoil," *Advances in Aerospace Engineering*, vol. 2014, 2014, doi: 10.1155/2014/504049.

[18] A. Voß, "Open and closed loop gust loads analyses for a flying wing configuration with variable longitudinal stability," *Aerospace Science and Technology*, vol. 89, pp. 1-10, 2019/06/01/ 2019, doi: 10.1016/j.ast.2019.03.049.

[19] P. Panagiotou, P. Kaparos, and K. Yakinthos, "Winglet design and optimization for a MALE UAV using CFD," *Aerospace Science and Technology*, vol. 39, pp. 190-205, 2014/12/01/ 2014, doi: 10.1016/j.ast.2014.09.006.

[20] Y. Zhang, L. Ye, and S. Yang, "Numerical study on flow fields and aerodynamics of tilt rotor aircraft in conversion mode based on embedded grid and actuator model," *Chinese Journal of Aeronautics*, vol. 28, pp. 93-102, 2015/02/01/ 2015, doi: 10.1016/j.cja.2014.12.028.

[21] H. Han, C. Xiang, B. Xu, and Y. Yu, "Aerodynamic performance and analysis of a hovering micro-scale shrouded rotor in confined environment," *Advances in Mechanical Engineering*, vol. 11, p. 1687814018823327, 2019, doi: 10.1177/1687814018823327.

[22] S. Sudhakar, N. Karthikeyan, and L. Venkatakrishnan, "Influence of leading edge tubercles on aerodynamic characteristics of a high aspect-ratio UAV," *Aerospace Science and Technology*, vol. 69, pp. 281-289, 2017/10/01/ 2017, doi: 10.1016/j.ast.2017.06.031.

[23] Z. Hui, Y. Zhang, and G. Chen, "Aerodynamic performance investigation on a morphing unmanned aerial vehicle with bio-inspired discrete wing structures," *Aerospace Science and Technology*, vol. 95, p. 105419, 2019/12/01/ 2019, doi: 10.1016/j.ast.2019.105419.

[24] D.-K. Kim, H.-I. Kim, J.-H. Han, and K.-J. Kwon, "Experimental Investigation on the Aerodynamic Characteristics of a Bio-mimetic Flapping Wing with Macro-fiber Composites," *Journal of Intelligent Material Systems and Structures*, vol. 19, pp. 423-431, 2008, doi: 10.1177/1045389x07083618.

[25] J.-H. Cho, "Experimental and numerical investigation of the power-on effect for a propeller-driven UAV," *Aerospace Science and Technology*, vol. 36, pp. 55-63, 2014/07/01/ 2014, doi: 10.1016/j.ast.2014.04.001.

[26] W. Boudaoud, T. Yahiaoui, B. Imine, and O. Imine, "Effect of an external vortex on the uav aerodynamic performances," *EPJ Web of Conferences*, vol. 25, p. 01104, 2012, doi: 10.1051/epjconf/20122501104.

[27] A. Boutemedjet, M. Samardžić, L. Rebhi, Z. Rajić, and T. Mouada, "UAV aerodynamic design involving genetic algorithm and artificial neural network for wing preliminary computation," *Aerospace Science and Technology*, vol. 84, pp. 464-483, 2019/01/01/ 2019, doi: 10.1016/j.ast.2018.09.043.

[28] S. Chang, A. Cho, S. Choi, Y. Kang, Y. Kim, and M. Kim, "Flight testing full conversion of a 40-kg-class tilt-duct unmanned aerial vehicle," *Aerospace Science and Technology*, vol. 112, p. 106611, 2021/05/01/ 2021, doi: 10.1016/j.ast.2021.106611.

[29] N. S. Hariharan, T. A. Egolf, and L. N. Sankar, "Simulation of Rotor in Hover: Current State, Challenges and Standardized Evaluation," in *52nd Aerospace Sciences Meeting*, ed, 2014 doi.org/10.2514/6.2014-0041.

[30] D. C. Dugan, "Trust control of VTOL aircraft part deux," in *Decennial, San Francisco, CA, AHS Aeromechanics Specialists' Conference*," 2014.

[31] P. Panagiotou, P. Kaparos, C. Salpingidou, and K. Yakinthos, "Aerodynamic design of a MALE UAV," *Aerospace Science and Technology*, vol. 50, pp. 127-138, 2016/03/01/ 2016, doi: 10.1016/j.ast.2015.12.033.

[32] L. Gao, C. Li, H. Jin, Y. Zhu, J. Zhao, and H. Cai, "Aerodynamic characteristics of a novel catapult launched morphing tandem-wing unmanned aerial vehicle," *Advances in Mechanical Engineering*, vol. 9, p. 1687814017692290, 2017, doi: 10.1177/1687814018823327.